Structural Monitoring and Maintenance, *Vol. 12, No. 1* (*2025*) *51-69*
https://doi.org/10.12989/smm.2025.12.1.051

Experimental investigation and numerical analysis of rotational deformation amplification friction self-centering brace

De-Bin Wang*, Ping-Fan Zhang[a], Shi-Peng Wang[b] and Qi-Yan Tan[c]

School of Traffic Engineering, Dalian Jiaotong University, Dalian 116028, China

(*Received September 3, 2024, Revised October 10, 2024, Accepted October 15, 2024*)

Abstract. This study presents a novel self-centering rotational deformation amplification function brace (RDAF-SCB) that is based on the bridge amplification working mechanism. Compared with conventional brace, RDAF-SCB can solve the problem that the conventional self-centering brace has insufficient energy dissipation ability and the deformation amplification damper lacks self-centering function. This paper introduces the basic structure and working mechanism of RDAF-SCB, and conducts low-cycle reversed loading tests on 6 groups of RDAF-SCB specimens under different working conditions to obtain and compare the key performance data of RDAF-SCB, including bearing capacity and hysteretic curve. A numerical simulation is conducted to analyze the influence of key factors on the mechanical behavior of the RDAF-SCB. The results indicate that the established finite element model agrees nicely with the test results, as the initial amplification angle decreases, the RDAF-SCB exhibits better energy dissipation capacity and fuller hysteresis curve. Compared with the model with an initial amplification angle of 45°, the RDAF-SCB with an initial amplification angle of 22.5°increases the force by 34.3%, the equivalent viscous damping ratio by 46.1%, and the maximal residual displacement ratio by 73.95% at the maximal forward displacement; when the initial amplification angle is unchanged, increasing the initial pre-pressure of the disc springs increases bearing capacity and decreases the residual deformation; with the increase of the preload force of the bolts, the energy dissipation capacity of the brace is enhanced and the residual deformation is slightly increased.

Keywords: deformation amplification; energy dissipation; residual deformation; self-centering

1. Introduction

Energy dissipation and damping technology can reduce the damage of seismic effects on the main body of the building, which is an important means of mitigating the structural seismic hazard by adding energy dissipation brace in the key parts of the structure (Zhu *et al.* 2021, Zhou *et al.* 2019). In order to reduce the residual deformation of the brace and facilitate the post-earthquake repair of the structure, a variety of new types of braces with self-centering function are proposed (Wang and Zhang 2019, Chen and Li 2020), the self-centering brace can reduce the residual deformation of the structure through its own self-centering capacity after the earthquake.

*Corresponding author, Professor, E-mail: wdb1215@163.com
[a]MA. Student
[b]Associate Professor, E-mail: caipeng9009@163.com
[c]MA. Student

http://www.techno-press.org/?journal=smm&subpage=7 ISSN: 2288-6605 (Print), 2288-6613 (Online)

Chrisropoulos *et al*. (2008) firstly proposed the concept of self-centering energy dissipation brace (SCEDB), which is mainly composed of a self-centering system and an energy dissipation system.

Based on the type of self-centering element, self-centering energy dissipation devices are mainly classified into spring-type self-centering devices (Liu *et al*. 2021, Wang and Zhou 2021), pre-stressing tendon type self-centering devices (Zhang *et al.* 2021) and shape memory alloy self-centering devices (Li and Wang 2020, Mokhtarnejad *et al*. 2023, Baikuntha *et al*. 2015). According to different energy dissipation methods, self-centering braces can be further classified into friction energy dissipation (Qiu *et al*. 2022, Liu and Sun 2021, Zhao *et al*. 2022), metal yielding energy dissipation (Zhao *et al*. 2023, Zhou *et al*. 2022) and viscous energy dissipation (Xu *et al*. 2018), etc. Guo *et al.* (2020) introduced an innovative self-centering cable-braced frame (SCCB) equipped with friction devices to enhance the seismic performance of existing reinforced concrete (RC) frame structures. They formulated a theoretical model for the restoring force of SCCB and conducted a parameter analysis to investigate the influence of cable stiffness and frictional forces on the hysteretic behavior of SCCB. Wang *et al*. (2021) proposed a new type of self-centering brace with disc springs as the self-centering material, introduced the working principle of the brace, and then carried out a full-scale experimental study on six full-scale specimens with different loading protocols. Xu *et al*. (2022) introduced an assembly-type pre-compressed spring self-centering energy-dissipating (A-PS-SCED) brace system, which employs a conical spring assembly to facilitate self-centering and incorporates a friction device for energy dissipation. They developed a theoretical model for the restoring force of the system and validated it through experimental investigations. Xu *et al*. (2021) proposed a new self-centering steel buckling restraint brace (SC-SBRB) consisting of two independent and complementary systems, the buckling restraint energy dissipation system and the pre-pressed disc spring self-centering system. Based on the working principle of SC-SBRB, a multifunctional self-centering hysteretic model (SCHM) is proposed, and the simulation results agree well with the predicted results, which verify the proposed SCHM's validity.

The deformation amplification damping device has been extensively investigated by numerous scholars both domestically and internationally. Li *et al.* (2021) proposed a new type of rotationally amplified viscoelastic damper, which utilizes the lever principle to multiply the relatively tiny corner deformation at the beam-column joint, and gives full play to the energy dissipation capacity of the damper by amplifying the corner deformation to achieve more ideal damping control. Wang *et al.* (2023) proposed a torsional friction self-centering brace with displacement amplification function, and conducted numerical simulation research and seismic response analysis of the double-column pier structure attached with the brace. The results show that SC-DARFB can further improve the damping energy dissipation capacity of the double-column pier with the reduction of the initial amplification angle. Huang *et al*. (2022) proposed a new self-centering large SMA damper, which amplifies the deformation through the lever principle, and gives full play to the energy dissipation capacity of SMA materials through the deformation amplification mechanism.

Based on the working mechanism of bridge mechanism amplification, a novel self-centering rotational deformation amplification function brace (RDAF-SCB) is proposed in this paper. The brace consists of a combined disc spring serving as the self-centering mechanism and a metal friction element functioning as the energy dissipation system, with both components arranged in parallel. This paper introduces the basic structure and working mechanism of RDAF-SCB, expounds the mechanism of brace force and deformation amplification of energy dissipation system, establishes the finite element model of the brace, and investigates the effects of initial

amplification angle, bolt tightening torque and pre-pressure of combined disc spring on the bearing capacity, energy dissipation capacity and self-centering performance of the brace.

2. The basic structure and working mechanism of RDAF-SCB

2.1 The basic structure of RDAF-SCB

The specific structure of RDAF-SCB is shown in Fig. 1. The brace comprises two components: a self-centering system and a friction energy dissipation system, which are interconnected in parallel via loading controls. The self-centering system consists of a restraining outer tube wall, transmission shaft, transmission shaft stopper, combined disc spring, disc spring stopper, and restraining end plates, as shown in Fig. 1(b). The transmission shaft is a stepped circular cross-section bar that serves as a guide for the disc spring. The external restraint sleeve of the self-centering system consists of the restraining outer tube wall and restraining end plates consolidated by high-strength bolts. The combined disc spring is inside the restraining outer tube wall and the combined disc spring is squeezed between the two baffle plates. The upper and lower projections of the outer tube wall restrict the movement of the disc spring plates, and the combined disc spring is constantly under pressure. Thus, the self-centering system is composed.

The energy dissipation system designed according to the bridge amplification principle, which is consists of an inner friction plate, an outer friction plate, friction plates, hinged pins and high-strength bolts evenly distributed in the ring direction. The energy dissipation system is symmetrically arranged on both sides of the self-centering system. The loading ends of the inner friction plate and the external friction plate are connected hinged to the loading control. The hinged pins at the loading end pass through the inner friction plate, the external friction plate and the friction plate to form a frictional energy dissipation system with four rotating friction surfaces, as shown in Fig. 1(c). The preload bolts are evenly arranged around the hinged pins, and the bolts surround the outside of the hinged pins to form multiple friction surfaces with the friction plates. Compared with the traditional rotating friction dampers, this arrangement can provide a larger and more stable friction torque for the RDAF-SCB under the same preloading force and friction factor to avoid stress concentration resulting from the localized pressure of the friction plates (American Institute of Steel Construction 2002).

2.2 Working mechanism of RDAF-SCB

The RDAF-SCB working mechanism is shown in Fig. 2. When the RDAF-SCB is in initial equilibrium, the pre-pressed combined disc spring is always under pressure by the combined forces of the transmission shaft and the external restraint sleeve. At the beginning, the transmission shaft and external restraint sleeve are jointly subjected to the initial pre-pressed and the energy dissipating system is not stressed. When the external load on the RDAF-SCB is less than the sum of the horizontal component force generated by the maximum static friction moment of the two energy dissipation systems and the initial pre-pressure of the self-centering system, the self-centering system is in an inactive state. At this time, the transmission shaft and the external restraint sleeve are in the elastic deformation state. When the force on the RDAF-SCB is greater than the sum of the horizontal component force of the energy dissipation system and the initial pre-pressure of the combined disc springs, the transmission shaft and the outer tube wall will move

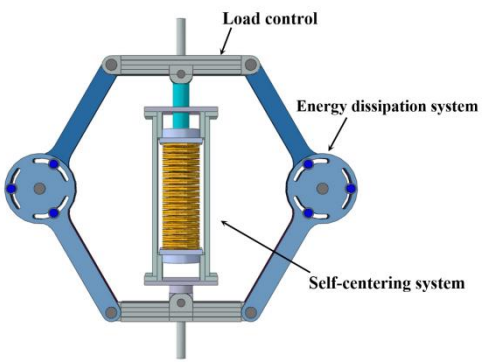

(a) Schematic of RDAF-SCB

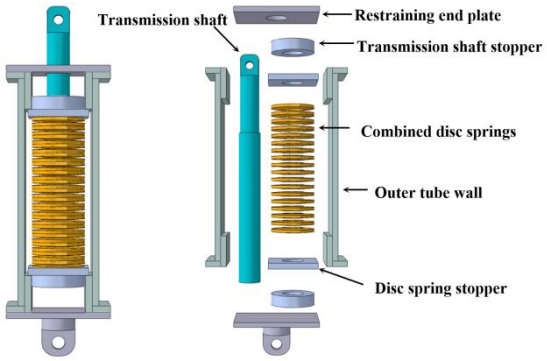

(b) The self-centering system

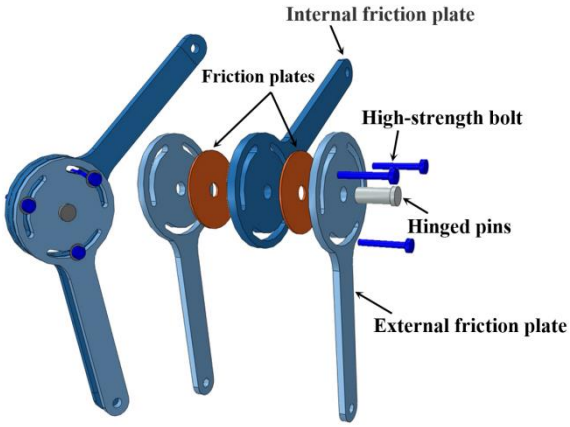

(c) The energy dissipation system

Fig. 1 Schematic diagram of the RDAF-SCB device

relative to each other, and the inner and external friction plates will rotate relative to each other and start frictional energy dissipation. When the force on the RDAF-SCB is decreased, the energy dissipation system will overcome the rotational frictional torque to return to the initial equilibrium state by the self-centering force provided by the combined disc spring.

2.3 Deformation amplification mechanism for energy dissipation systems

The force and deformation process of the RDAF-SCB energy dissipation system under external loading is shown in Fig. 3.

F_f and F'_f are classified as the horizontal component of the force transmitted to the loading control by the rotating friction plate when the RDAF-SCB is in tension or compression. d is the axial displacement of the RDAF-SCB. θ_0 is the initial amplification angle. $\Delta\theta$ is the change of the initial amplification angle of the rotating friction plate. φ is the relative angle of rotation of the inner and outer friction plates, and $\varphi/2 = \Delta\theta$. θ is the actual amplification angle after loading of the RDAF-SCB. L is the effective length of the rotating friction plate; M is the friction moment generated by the unilateral energy dissipation system. When RDAF-SCB is loaded, point A always moves along the axis of RDAF-SCB, and point B moves in a straight line along the vertical

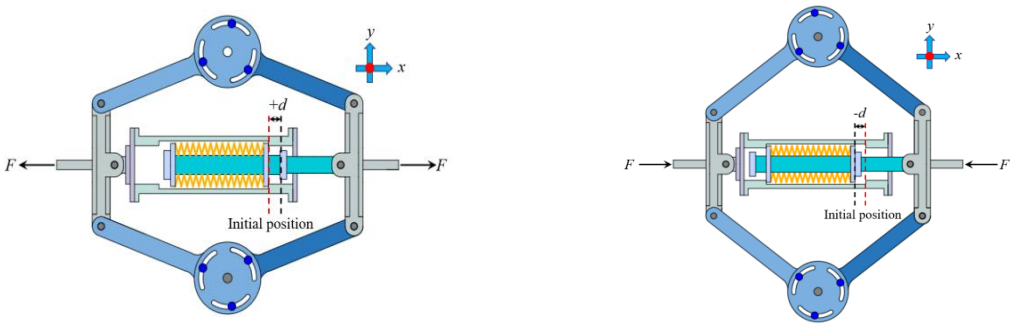

(a) The tension state (b) The compression state

Fig. 2 Working mechanisms of the RDAF-SCB

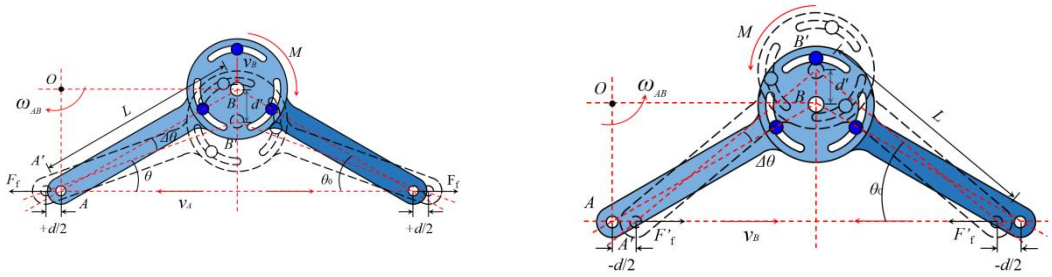

(a) The tension state (b) The compression state

Fig. 3 Mechanism diagram of deformation amplification in RDAF-SCB energy-dissipation system

direction of RDAF-SCB axis. Therefore, the inner and external friction plate motion mode are plane motion, the points on the external friction plate (AB) can be regarded as translating with point A and rotating around point A. Therefore, the velocity perpendiculars of points A and B can be used to obtain the instantaneous center of *O*. From the method of instantaneous center of gravity, it can be seen that the velocities v_A and v_B at the points A and B of the external friction plate and the angular velocity ω_{AB} of the external friction plate are related as follows:

$$\omega_{AB} = \frac{v_A}{L\sin\theta} = \frac{v_B}{L\cos\theta} \tag{1}$$

During the loading process, the initial amplification angle change of both the RDAF-SCB's load-bearing ends is $\Delta\theta$, the axial displacement is $d/2$, and the vertical displacement of the center point of the hinged pin hole (point B) is d'. From the triangle interior angle sum is always 180°, it can be seen that the angular displacement φ of the external friction plate relative to the inner friction plate is two times of $\Delta\theta$. According to the nature of rigid body plane motion, the angular velocity of the plane figure rotating around the base point is independent of the choice of the base point, so the angular velocity of the external friction plate (AB) rotating around point A is ω_{AB}. Let the loading time t, since the deformation of RDAF-SCB is small compared to its size, φ and $\Delta\theta$ can be expressed as

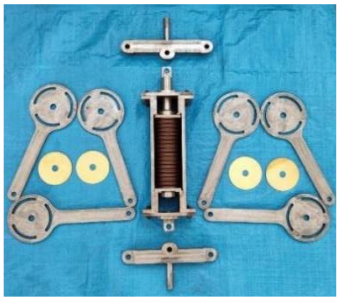

Fig. 4 Basic structure of RDAF-SCB

$$\Delta\theta = \frac{\varphi}{2} = \omega_{AB} t = \frac{v_A}{L\sin\theta} t \tag{2}$$

Since there exists the following relationship between the RDAF-SCB axial displacement and the velocity at point A of the external friction plate

$$\frac{d}{2} = v_A t \tag{3}$$

Substituting Eq. (3) into Eq. (2)

$$\varphi = 2\Delta\theta = \frac{d}{L\sin\theta} \tag{4}$$

It can be seen that the relative angle φ of the inner and external friction plates is directly related to the amplification angle θ. By modifying the initial amplification angle θ_0, the angle amplification times of the inner and external friction plates of the energy dissipation system of the RDAF-SCB can be adjusted, which will improve the energy dissipation performance of the RDAF-SCB.

3. RDAF-SCB hysteretic behavior tests

3.1 Designed test specimens

The physical diagram of each part of the test specimen is shown in Fig. 4, the assembly of the structure of the device shown in Fig. 5. During the test process, the RDAF-SCB amplification angle changes continuously with the displacement and the reset ratio changes as well. The reset ratio is the ratio of the initial pre-pressed force of the disc springs to the friction force provided by the energy dissipation devices. The initial amplification angle decreases, the load generated by the energy-dissipation system in the brace axis increases, the reset ratio will decrease, and the residual deformation will increase. In this paper, the effect of initial amplification angle on the mechanical properties of the device is mainly considered. Six test conditions are designed, and the detailed design is shown in Table 1.

Table 1 The condition design of braces

Loading case	θ_0/(°)	F_f/kN	P_0/kN	Reset ratio
RDAF-SCB-1	45	3.1	—	—
RDAF-SCB-2	30	5.0	—	—
RDAF-SCB-3	45	3.1	8	1.3
RDAF-SCB-4	45	3.6	8	1.1
RDAF-SCB-5	30	5.0	13	1.3
RDAF-SCB-6	30	5.9	13	1.1

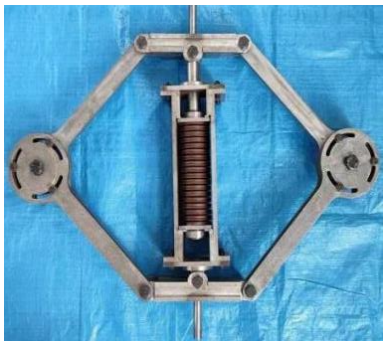

Fig. 5 Assembly diagram of RDAF-SCB

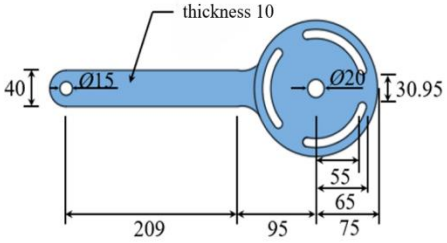

(a) Dimensions of outer friction plates

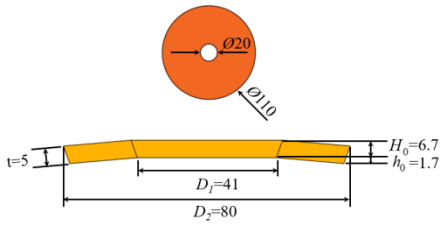

(b) Dimensions of disc spring

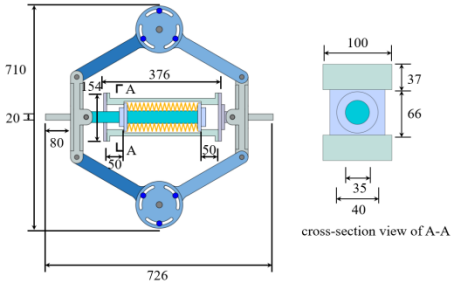

(c)The overall dimensions diagram

Fig. 6 The dimensions of the RDAF-SCB bracing system (mm)

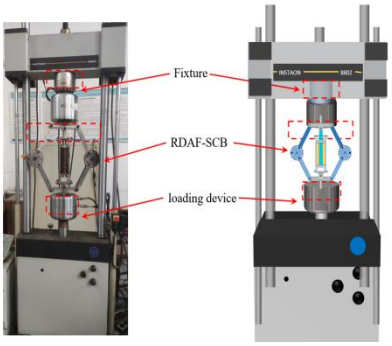

Fig. 7 Test setup

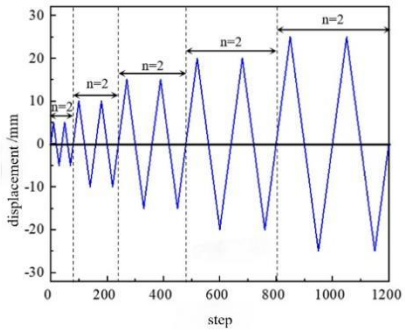

Fig. 8 Loading protocol

The basic dimensional parameters of the constituent parts of RDAF-SCB at θ_0 = 30° are shown in Fig. 6, with the same dimensions of the inner and external friction plates. When θ_0 = 45°, the device simply adjusts the effective length of the inner and external friction plates to 277 mm, and the rest of the constituent parts are consistent with the dimensions of the parts at θ_0 = 30°. According to GB/T1972-2005 “Disc spring” specification (2005) selection of A series of disc springs, two single-layer pairs together as a group, a total of 17 groups, disc spring size as shown in Fig. 6(b), among them, D_1 and D_2 are the inner diameter and external diameter of the disc spring; H_0 and h_0 are the calculated height and deformation of a single disc spring compression level; t is the thickness of a single disc spring. Brass is chosen as the friction material, transmission shafts are made of 40Cr steel, the preload bolt is M12.9 grade, and the rest of the parts are made of Q345B grade steel. In order to ensure that the bolt preload force acts stably on the surface of the friction plate, the bolt holes of the inner and external friction plates are processed as curved long holes, and the bolts are attached to the surface of the friction plate on the side of the spring spacer.

3.2 Testing device and loading protocol

In this test, INSTRON-8802 fatigue testing machine was used to carry out cyclic loading of the specimen, with a maximum load of 250 kN and a displacement stroke of ±75 mm, and the test setup as shown in Fig. 7 The initial loading displacement amplitude of each condition was 5 mm,

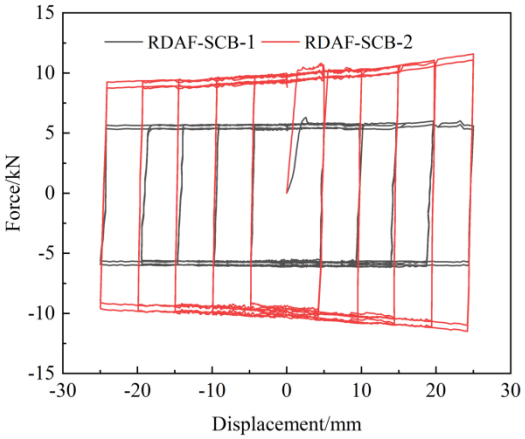

Fig. 9 Hysteresis curves of the RDAF-SCB

Table 2 The key mechanical properties of braces

Loading case	Yield displacement /mm	Yield load /kN	Ultimate load (tension and compression)/kN	Maximum tensile/compressive load ratio
RDAF-SCB-1	-	-	6.31/-5.86	1.029
RDAF-SCB-2	-	-	11.59/-10.99	1.055
RDAF-SCB-3	2.68	16.13	39.97/-40.09	1.003
RDAF-SCB-4	2.88	17.52	42.08/-41.96	1.002
RDAF-SCB-5	2.97	23.81	51.74/-49.96	1.035
RDAF-SCB-6	3.23	25.84	53.34/-51.69	1.032

and the subsequent displacement amplitude was taken as the displacement increment of 5 mm, until the displacement was loaded to 25 mm to end the loading. At each level of displacement amplitude, two cycles of repetitive cyclic loading are administered. The loading protocol is shown in Fig. 8. The displacement-controlled loading mode is used for loading with a loading frequency of 0.05 Hz.

3.3 Test results

When the brace is not equipped with self-centering system, the hysteresis curves of specimens RDAF-SCB-1 and RDAF-SCB-2 are shown in Fig. 9, which are full and show good energy dissipation ability and excellent “rigid-plastic” characteristics. The hysteresis curve exhibits pronounced asymmetric characteristics. Based on the amplification mechanism previously discussed, when the frictional energy dissipation system generates a specific friction moment M, the friction moment produced by both the internal and external friction plates along the axial direction of the brace will increase exponentially for amplification angles $\theta < 45°$. Furthermore, during tensile loading of the brace, as displacement increases, the amplification angle θ will

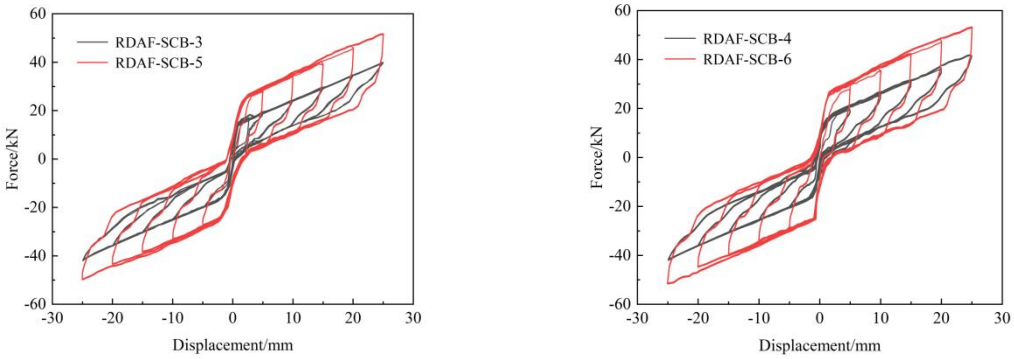

(a) RDAF-SCB-3 and 5 (b) RDAF-SCB-4 and 6

Fig. 10 Hysteretic curves of the RDAF-SCB

decrease, resulting in an escalation of load on the brace. As the brace is compressed, the amplification angle θ increases with the displacement of the brace. Consequently, this results in a reduction of the frictional energy dissipation system's friction moment along the axial direction of the brace, thereby giving rise to pronounced asymmetric characteristics in the hysteresis curve. As illustrated in Table 2, the hysteresis curve of specimen RDAF-SCB-2 exhibits a larger area compared to specimen RDAF-SCB-1, which has an initial amplification angle of θ=45°. This indicates a significant enhancement in energy dissipation capacity and an increase in maximum load by 83.7%. Such findings demonstrate improved bearing capacity under identical displacement amplitudes. Additionally, the ratio of maximum tensile to compressive loads shows a slight increase to 1.055, primarily attributed to the more pronounced effect of changing the initial amplification angle to θ_0=30° with increasing displacement.

The introduction of the self-centering system is illustrated by the hysteretic curves presented in Fig. 10. During reverse loading, brief approximate plateaus were observed, primarily attributed to the transition of contact surfaces between the axle holes and pins in the connecting components from forward to reverse contact upon brace reverse loading. Additionally, processing gaps exist between these components; thus, during reverse loading, it is essential to first compensate for the machining clearance between the pins and axle holes before they can be subjected to reloading. In comparison to the initial amplification angle of θ=45° for specimens RDAF-SCB-3 and RDAF-SCB-4, specimens RDAF-SCB-5 and RDAF-SCB-6, which maintain a consistent reset ratio at θ=30°, exhibit increases in yield load and maximum load of 47.6%、47.5% and 29.4%、26.8%, respectively. This indicates that the initial amplification angle significantly influences the yield load of the brace; primarily because the load sustained by the self-centering system operates independently from the amplification angle of the energy dissipation mechanism, thereby constituting a larger proportion of the total support load. Furthermore, as displacement amplitude escalates, while axial force generated by the energy dissipation system remains relatively constant, forces borne by the self-centering system increase rapidly with rising displacement amplitudes.

The incorporation of a self-centering system significantly mitigated the residual deformation of the brace. When the initial amplification angles θ_0 are set at 45° and 30°, the maximum residual deformation of the brace across all operational conditions remains below 10% of its peak loading displacement, indicating that RDAF-SCB exhibits commendable self-centering performance. With a constant initial pre-pressure in the combined disc spring, it is observed that a smaller initial

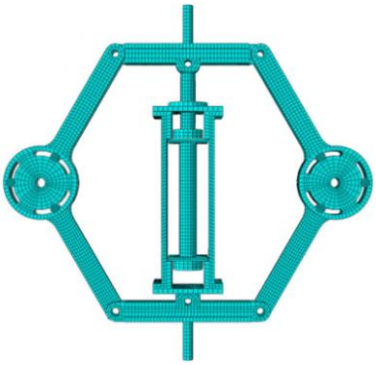

Fig. 11 The finite element model

amplification angle results in an increase in horizontal force generated by the energy dissipation system. Consequently, this horizontal force may surpass the initial pre-pressure of the combined disc spring, leading to an escalation in residual deformation within the device. Furthermore, when maintaining a constant initial amplification angle θ_0 for RDAF-SCB, it is evident that as the reset ratio increases, there is a corresponding decrease in residual deformation. Calculations reveal that, under identical parameter conditions, the cumulative energy dissipation of specimens RDAF-SCB-1 and RDAF-SCB-2, which lack a self-centering system, is lower than that of specimens RDAF-SCB-3 and RDAF-SCB-5. This observation arises from the fact that, while maintaining a constant energy dissipation system, the frictional force between the combined disc springs and the transmission shaft within the self-centering system increases, thereby augmenting the energy dissipation capacity of the brace.

4. Numerical simulation and verification

4.1 Numerical simulation

The refined model of RDAF-SCB was established based on ABAQUS, as shown in Fig. 11. The dimensions of each component of the numerical model are the same as those of the test specimen, and each component adopts eight-node linear hexahedral reduced integral solid unit (C3D8R). The mesh sizes of the loading control, inner and outer friction plates, transmission shaft, transmission shaft stopper, and restraint sleeve are uniformly set at 7 mm. These components are constructed from Q345 grade steel, which exhibits a yield strength of f_y = 345 MPa, a tensile strength of f_u = 500 MPa, an elastic modulus of E = 206 GPa, and a Poisson's ratio of v = 0.3. Additionally, the mesh size for the friction plates is specified as 2.5 mm. The surfaces of the preloaded bolts and the inner and outer friction plates are configured for face-to-face contact. The tangential interactions between the preloaded bolts and the surfaces of both inner and outer friction plates are modeled using a 'penalty function' friction type, while normal interactions are represented by a 'hard contact' approach. The friction coefficient between the friction plate and the inner and external friction plates is 0.34, and hard contact is still used in the normal direction. To mitigate excessive contact that may hinder the model's convergence, a hinge command is established between the internal apertures of the inner and outer friction plates to facilitate

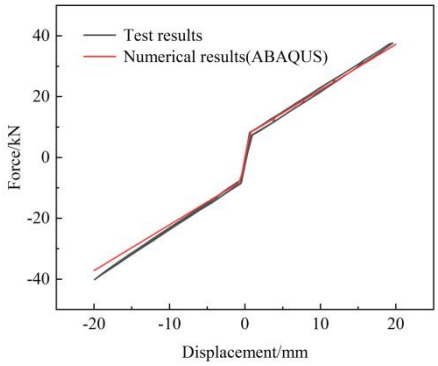

Fig. 12 Hysteresis curve of disc springs

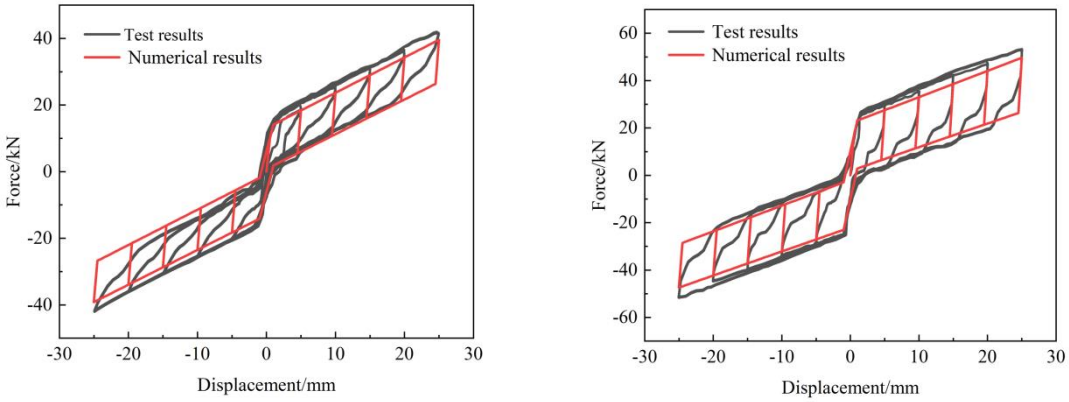

(a)RDAF-SCB-4 (b) RDAF-SCB-6

Fig. 13 Comparison of the hysteretic curves between test and numerical simulation

rotational interaction among all three components. The preload bolts, which exert normal lateral pressure, are represented by linear elastic spring units, with initial preload pressure applied through a predetermined reference length. To minimize contact and enhance computational efficiency, the combined disc spring within the self-centering system is modeled as a nonlinear spring unit; its stiffness and initial preload are characterized by defining axial stiffness and reference length. The simulation results for the reset system are illustrated in Fig. 12, demonstrating strong alignment with test results.

4.2 Numerical model verification

Fig. 13 presents a comparison of the hysteresis curves derived from both RDAF-SCB-4 and RDAF-SCB-6 tests alongside their corresponding simulations. The figure illustrates that the hysteresis curves obtained through finite element simulations align closely with the experimental results. Notably, the load values and post-yield stiffness recorded at each displacement amplitude during testing exceed those predicted by numerical simulations, whereas the unloading stiffness is

Table 3 Design parameter values of RDAF-SCB

Specimens	Design parameters	Initial amplification angle	Bolt tightening torque / N•m	Initial pre-pressure of disc spring /kN	Reset ratio
RDAF-SCB-1	Initial amplification angle	22.5°	20	12.97	1.2
RDAF-SCB-2		30°	20	10.00	1.2
RDAF-SCB-3		37.5°	20	8.21	1.2
RDAF-SCB-4		45°	20	7.38	1.2
RDAF-SCB-5	Bolt tightening torque	30°	25	8	0.77
RDAF-SCB-6		30°	20	8	0.96
RDAF-SCB-7		30°	15	8	1.29
RDAF-SCB-8	Initial pre-pressure of disc spring	30°	25	8	0.77
RDAF-SCB-9		30°	25	12	1.16
RDAF-SCB-10		30°	25	16	1.54

found to be lower than their simulated counterparts. The reasons for this phenomenon are as follows: 1) the simulation process does not account for the combined effects of the disc spring, transmission shaft, and friction interactions among the connecting components; 2) machining gaps and errors present between the constituent parts of the specimen contribute to a marginal reduction in unloading stiffness.

5. Parameter analyses

5.1 Construction parameter

A parametric analysis is carried out based on the validated finite element model to investigate the effects of parameter variations on the hysteresis performance of RDAF-SCB. The key parameters include: initial amplification angle, bolt tightening torque, and initial pre-pressure of disc spring. A total of 10 RDAF-SCBs are designed, and the detailed design parameters are shown in Table 3.

5.2 Initial amplification angle

To investigate the influence of the initial amplification angle on the hysteresis performance of RDAF-SCB, we selected initial amplification angles of 22.5°, 30°, 37.5°, and 45°. A finite element model of the brace was developed, and the resulting hysteresis curve from simulation is presented in Fig. 14. The load values at which RDAF-SCB achieves maximum displacement for initial amplification angles of 22.5°, 30°, 37.5°, and 45° are recorded as 52.8 kN, 44.9 kN, 41.1 kN, and 39.3 kN, respectively. At maximum forward displacement, RDAF-SCB-1, RDAF-SCB-2, and RDAF-SCB-3 with initial amplification angles of 22.5°, 30°, and 37.5° exhibit improvements in load capacity by approximately 34.3%, 14.2%, and 4.6% compared to models with an initial amplification angle of 45°. This finding indicates that a reduction in the initial amplification angle significantly enhances the load capacity effect of RDAF-SCB; both yield loads and maximum

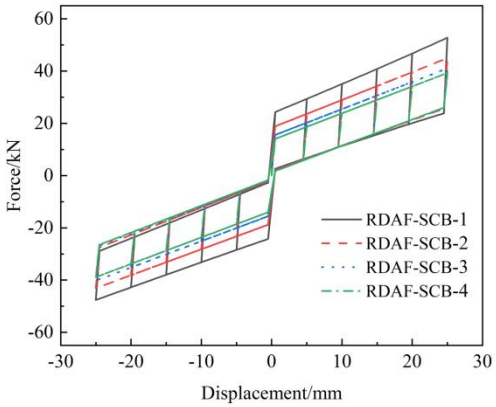

Fig. 14 Hysteresis curves of the RDAF-SCB-1~4

loads progressively increase while also enlarging the area enclosed by the hysteresis curve during plastic deformation stages—thereby augmenting energy dissipation capabilities as well. Furthermore, when increasing the initial amplification angle while maintaining a constant reset ratio, residual deformation remains relatively unchanged across all specimens which demonstrate commendable self-centering performance.

The equivalent viscous damping ratio is a critical parameter for assessing the energy dissipation capacity of structures in the context of earthquake resistance within engineering applications. Fig. 15 illustrates the equivalent viscous damping ratios of braces at various initial amplification angles. It is evident that the equivalent viscous damping ratio increases rapidly with displacement, followed by a gradual decline, ultimately stabilizing overall energy dissipation. Notably, when comparing the RDAF-SCB-4 brace model with an initial amplification angle of 45° to the RDAF-SCB-1 model with an initial amplification angle of 22.5°, there is a significant increase of 46.1% in the maximum forward displacement for the latter. Furthermore, as the initial amplification angle decreases, there is a pronounced increase in both the equivalent viscous damping ratio and energy dissipation capacity of the brace, thereby enhancing its performance under identical displacement amplitudes or minor deformations.

5.3 Bolt tightening torque

The tightening torque of the bolts significantly influences the energy dissipation capacity of the brace. By setting the initial amplification angle at 30° and varying the bolt tightening torques to 25, 20, and 15 N•m respectively, we obtained the hysteresis curves for each brace under these different conditions, as illustrated in Fig. 16. The results indicate that an increase in bolt tightening torque enhances both yield load and maximum load capacities of RDAF-SCB, thereby improving its performance across various loading amplitudes. Specifically, when subjected to bolt tightening torques of 25 N•m, 20 N•m, and 15 N•m respectively, RDAF-SCB exhibited bearing capacities of 45.3 kN, 42.9 kN, and 40.5 kN at maximum displacement. At this peak forward displacement stage, specimens RDAF-SCB-5 and RDAF-SCB-6 demonstrated increases in load values by approximately 11.9% and 5.9%, compared to their counterpart braced model with a bolt tightening moment of only 15 N•m. Furthermore, it is evident that higher bolt tightening torque results in a

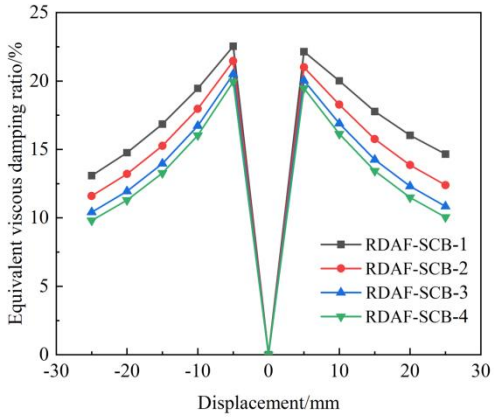

Fig. 15 The equivalent viscous damping ratio of RDAF-SCB-1~4

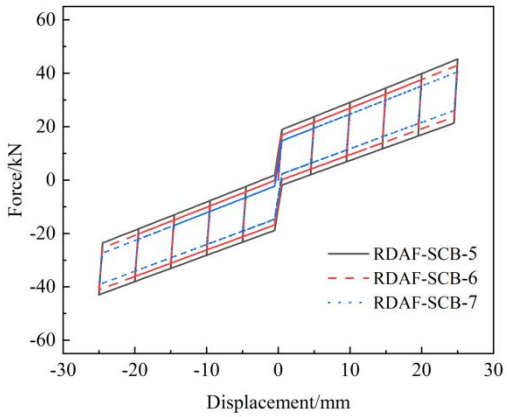

Fig. 16 Hysteresis curves of the RDAF-SCB-5~7

more pronounced hysteresis curve for RDAF-SCB along with improved energy dissipation capacity; concurrently leading to an increase in initial sliding load for the brace itself. Additionally, residual displacement was observed to rise alongside increasing bolt tightening torque while exhibiting a slight reduction in reset capacity.

5.4 Initial pre-pressure of disc spring

The initial preload of the disc spring plays a crucial role in determining the self-centering efficacy of the brace. By setting the initial amplification angle at 30° and varying the initial pre-pressure of the disc spring to 8 kN, 12 kN, and 16 kN, we compared the hysteresis curves for each configuration as illustrated in Fig. 18. The analysis reveals that while there are minimal differences in the envelope areas of these hysteresis curves across all three conditions, the initial pre-pressure significantly influences the initial sliding force of the RDAF-SCB. As the initial pre-pressure increases, so does the brace's initial sliding force; however, its energy dissipation capacity remains

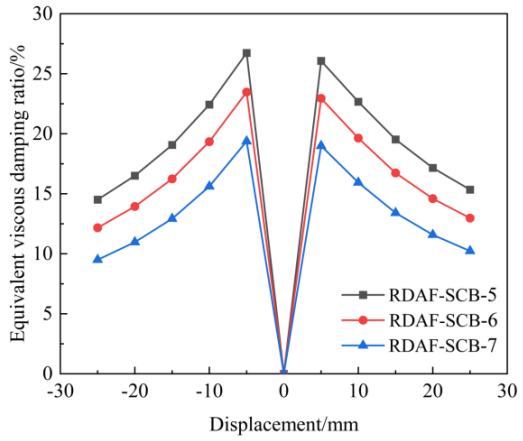

Fig. 17 The equivalent viscous damping ratio of RDAF-SCB-5~7

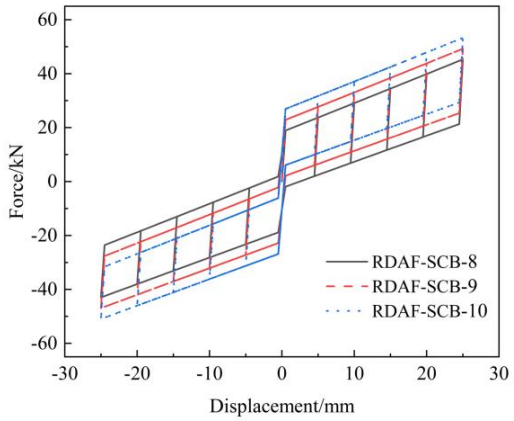

Fig. 18 Hysteresis curves of the RDAF-SCB-8~10

constant. Notably, both bearing capacity and residual deformation exhibit improvements: bearing capacity approximately equals this increment in pre-pressure while residual deformation decreases markedly, thereby enhancing self-centering performance.

Fig.19 illustrates the equivalent viscous damping ratio of the brace under varying initial pre-pressures. As displacement increases, the equivalent viscous damping ratio initially rises before gradually declining, while overall energy dissipation remains stable. In comparison to the RDAF-SCB-8 brace model with a disc spring initial pre-pressure of 8 kN, the equivalent viscous damping ratio for the RDAF-SCB-10 model with an initial pre-pressure of 16 kN is reduced by 25.58% at the maximum positive amplitude. Notably, higher pre-pressure correlates with a lower equivalent viscous damping ratio and a slight decrease in energy dissipation efficiency of the brace. This indicates that enhancing self-centering capability can be effectively achieved through increased initial pre-pressure; thus, both initial pre-pressure and its impact on energy dissipation efficiency should be comprehensively considered during brace design.

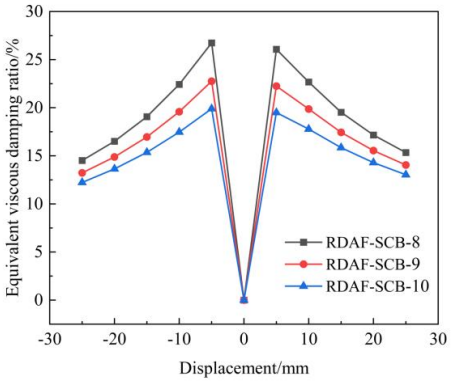

Fig. 19 The equivalent viscous damping ratio of RDAF-SCB-8~10

6. Conclusions

Based on the principle of bridge amplification, an RDAF-SCB with rotational deformation amplification function is proposed in this paper. The fundamental structure and operational mechanism of the RDAF-SCB are elaborated in detail. Experimental investigations into the mechanical properties of the RDAF-SCB under cyclic loading are conducted. A finite element model for the brace is developed, and an analysis of key parameters influencing its performance is performed. The principal conclusions drawn from this study are as follows:

- In comparison to an RDAF-SCB lacking a deformation amplification feature, when the initial amplification angle θ_0=30°, both yield load and maximum load exhibited increases of 47.6% and 29.4%, respectively, indicating that reducing the initial amplification angle can significantly enhance both bearing capacity and energy absorption performance.
- Utilizing ABAQUS software, simulations were conducted on combined disc springs and tightening bolts subjected to initial deformation conditions; hard contact was applied in normal directions while penalty function contact mode was employed tangentially. The finite element model for RDAF-SCB was established successfully, with simulated hysteretic curves aligning closely with experimental results—effectively reflecting key mechanical characteristics of the brace.
- It was observed that both energy dissipation capacity and equivalent viscous damping ratio for RDAF-SCB increased alongside bolt tightening force, although residual deformation showed only slight increments. Furthermore, as initial pre-pressure within the brace increased—with corresponding enhancements in reset ratios—the energy dissipation performance remained relatively stable; however, there was a minor reduction in equivalent viscous damping ratio while improvements were noted in bearing capacity and reset functionality.

Acknowledgments

This research was supported by Key Laboratory of Building Structural Retrofitting & Underground Space Engineering (Shandong Jianzhu University), (Grant No. MEKL202309).

References

American Institute of Steel Construction. (2002), Seismic provisions for structural steel buildings (No. 2). *American Institute of Steel Construction*.

Baikuntha, S., Michael, R.J. and Osman, O.E. (2015), "A superelastic viscous damper for enhanced seismic performance of steel moment frames", *Eng. Struct.*, **105**, 152-164. https://doi.org/10.1016/j.engstruct.2015.10.005.

Chen, Z. and Li, W. (2020), "Experimental study on passive control of buildings using self-centering braces", *Struct. Monit. Maint.*, **7**(3), 245-260. https://doi.org/10.12989/smm.2020.7.3.245.

Christopoulos, C., Tremblay, R., Kim, H.J. and Lacerte, M. (2008), "Self-centering energy dissipative bracing system for the seismic resistance of structures: Development and validation", *J. Struct. Eng.*, **134**(1), 96–107. https://doi.org/10.1061/(ASCE)0733-9445(2008)134:1(96).

GB/T 1972-2005. (2005), Disc spring [S]. *Beijing: China Standards Press*.

Guo, T., Wang, J., Song, Y., Xuan, W. and Chen, Y. (2020), "Self-centering cable brace with friction devices for enhancing seismic performance of RC frame structures", *Eng. Struct.*, **207**, 110187. https://doi.org/10.1016/j.engstruct.2020.110187.

LI, D.B. and Zhou, Y. (2022), "A force-resisting rotary friction damper (RFD): Verification and comparison with traditional RFD", *Eng. Struct.*, **273**,115015.

Li, H.N., LI, Y.L., Huang, Z. and Fu, X. (2021), "Experimental study on the properties of a new rotation-magnified viscoelastic damper", *Eng. Mech.*, **38**(2), 134-145.

Li, Y. and Wang, Z. (2020), "Passive control of high-rise buildings using self-centering braces and friction dampers", *Struct. Eng. Mech.*, **74**(6), 723-737. https://doi.org/10.12989/sem.2020.74.6.723.

Liu, J.W., Qiu, C.X. and Du, X.L. (2021), "Analysis of self-centering support parameters including replaceable energy-dissipating steel plate", *J. Beijing Univ. Technol.*, **47**(4), 374-382.

Liu, J. and Sun, Q. (2021), "Performance evaluation of a novel amplified friction damper for seismic mitigation", *Smart Struct. Syst.*, **27**(2), 189-202. https://doi.org/10.12989/sss.2021.27.2.189

Mokhtarnejad, N., Garmeh, V., Shariatmadar, H. and Askariani, S.S. (2023), "Numerical study of a novel SMA-based self-centering beam-to-column connection", *Structures*, **47**, 1033-1049. https://doi.org/10.1016/j.istruc.2022.11.128.

Qiu, C.X., Liu, J. and Du, X.L. (2022), "Cyclic behavior of SMA slip friction damper", *Eng. Struct.*, **250**, 113407. https://doi.org/10.1016/j.engstruct.2021.113407.

Wang, D.B., He, J., Sun, Z.G., et al. (2023), "Friction fail-safe bracing with displacement amplification function and its application in double-column bridge pier", *J. Vib. Shock*, **42**(2), 51-59. https://doi.org/10.13465/j.cnki.jvs.2023.02.007.

Wang, W., Fang, C., Shen, D. et al. (2021), "Performance assessment of disc spring-based self-centering braces for seismic hazard mitigation", *Eng. Struct.*, **242**, 112527. https://doi.org/10.1016/j.engstruct.2021.112527.

Wang, X. and Zhang, Y. (2019), "Seismic performance of structures equipped with self-centering braces and viscous dampers", *Earthq. Struct.*, **18**(4), 401-415. https://doi.org/10.12989/eas.2019.18.4.401.

Wang, Y. and Zhou, Y. (2021), "Self-centering braces with friction dampers: experimental and numerical studies", *Earthq. Struct.*, **20**(3), 301-315. https://doi.org/10.12989/eas.2021.20.3.301.

Xu, L.H., Xie, X.S. and Li, Z.X. (2018), "A self-centering brace with superior energy dissipation capability: Development and experimental study", *Smart Mater. Struct.*, **27**(9), 095017. https://doi.org/10.1088/1361-665X/aad5b0.

Xu, L., Chen, P. and Li, Z. (2021), "Development and validation of a versatile hysteretic model for pre-compressed self-centering buckling-restrained brace", *J. Constr. Steel Res.*, **177**, 106473. https://doi.org/10.1016/j.jcsr.2020.106473.

Xu, L., Lin, Z. and Xie, X. (2022), "Assembled self-centering energy dissipation braces and a force method-based model", *J. Constr. Steel Res.*, **190**, 107121. https://doi.org/ 10.1016/j.jcsr.2021.107121.

Zhang, C.Z., Guo, X.N., Zhu, S.J., *et al.* (2021), "Hysteretic performance of prefabricated self-centering

buckling restraint support", *J. Tongji Univ., (Natural Science Edition)*, **49**(1), 8-19.
Zhao, G., Ma, Y., Yang, Z., Wang, Q. and Li, Y. (2022), "Friction mechanism and experimental investigation of the response-amplified friction damper", *Struct. Control Health Monit.*, **29**(7), e2953. https://doi.org/10.1002/stc.2953.
Zhao, J., Zhang, J., Song, J., Zhou, Y., Bai, J. and Yu, H. (2023), "Sliding gusset connections for improved seismic performance of BRB-RC frame: Damage-control design and subassemblage tests", *Eng. Struct.*, **282**, 115828. https://doi.org/ 10.1016/j.engstruct.2023.115828.
Zhou, X., Sun, T., Sun, B., Ma, N. and Ou, J. (2022), "Vibration-reduction strategy for high-rise braced frame using viscoelastic-yielding compounded BRB", *Buildings*, **12**(8), 1159. https://doi.org/10.3390/buildings12081159.
Zhou, Y., Shang, C.H. and Zhang, C. (2019), "Research and application progress of energy dissipation and shock absorption technology", *Build. Struct.*, **19**, 33-48. https://doi.org/10.19701/j.jzjg.2019.19.005.
Zhu, L.H., Li, G. and Dong, Z.Q. (2021), "Dynamic test and numerical simulation on avoiding the weak-story failure mechanism in structures using LSFDs", *Steel Compos. Struct.*, **40**(2), 175-191. https://doi.org/10.12989/scs.2021.40.2.175.